Electronically excited and ionized states of the CH_2CH_2OH radical: A theoretical study

B. Karpichev,[a] L. Koziol, K. Diri, H. Reisler, and A. I. Krylov[b]
Department of Chemistry, University of Southern California, Los Angeles, California 90089-0482, USA

(Received 17 December 2009; accepted 15 February 2010; published online 19 March 2010)

The low lying excited electronic states of the 2-hydroxyethyl radical, CH_2CH_2OH, have been investigated theoretically in the range 5–7 eV by using coupled-cluster and equation-of-motion coupled-cluster methods. Both dissociation and isomerization pathways are identified. On the ground electronic potential energy surface, two stable conformers and six saddle points at energies below ~900 cm^{-1} are characterized. Vertical excitation energies and oscillator strengths for the lowest-lying excited valence state and the 3s, $3p_x$, $3p_y$, and $3p_z$ Rydberg states have been calculated and it is predicted that the absorption spectrum at ~270–200 nm should be featureless. The stable conformers and saddle points differ primarily in their two dihedral coordinates, labeled d_{HOCC} (OH torsion around CO), and d_{OCCH} (CH_2 torsion around CC). Vertical ionization from the ground-state conformers and saddle points leads to an unstable structure of the open-chain $CH_2CH_2OH^+$ cation. The ion isomerizes promptly either to the 1-hydroxyethyl ion, CH_3CHOH^+, or to the cyclic oxirane ion, $CH_2(OH)CH_2^+$, and the Rydberg states are expected to display a similar behavior. The isomerization pathway depends on the d_{OCCH} angle in the ground state. The lowest valence state is repulsive and its dissociation along the CC, CO, and CH bonds, which leads to CH_2+CH_2OH, CH_2CH_2+OH, and $H+CH_2CHOH$, should be prompt. The branching ratio among these channels depends sensitively on the dihedral angles. Surface crossings among Rydberg and valence states and with the ground state are likely to affect dissociation as well. It is concluded that the proximity of several low-lying excited electronic states, which can either dissociate directly or via isomerization and predissociation pathways, would give rise to prompt dissociation leading to several simultaneous dissociation channels. © *2010 American Institute of Physics*. [doi:10.1063/1.3354975]

I. INTRODUCTION

Hydroxyalkyl radicals play an important role in many atmospheric and combustion reactions, but relatively little is known about their excited electronic states and photodissociation dynamics, except for the two smallest members of the group, CH_2OH and CH_3CHOH.[1–12] The latter, 1-hydroxyethyl, is a structural isomer of the hydroxyethyl radical, and with the radical center placed on the carbon adjacent to the oxygen, it behaves similarly to the hydroxymethyl radical, CH_2OH. The 2-hydroxyethyl radical, CH_2CH_2OH, in which the unpaired electron is located on the outermost carbon, should have a different electronic structure. It is an intermediate in the $OH+C_2H_4$ reaction and has been stabilized at low temperatures.[1,2,13–19] There are several theoretical studies of the ground state of the neutral and the cation of CH_2CH_2OH,[2,20–22] but to the best of our knowledge there are no theoretical studies of its excited electronic states. Anastasi *et al.*[23] published a 300 K UV absorption spectrum of CH_2CH_2OH. It starts at about 260 nm (4.77 eV) and rises slowly toward shorter wavelengths, and it is featureless. In molecular beam experiments the radical was produced by photolysis of haloethanols,[24–27] and noticeable absorption at 266 nm (4.66 eV) was observed.[25,26]

The CH_2CH_2OH radical is interesting from both theoretical and experimental perspectives. Whereas the neutral species has a typical open chain configuration (see Fig. 1), the cation has no minima in this configuration. Instead, the Franck–Condon region has a saddle point which leads to the only two minima on the cation surface: a nonclassical cyclic bridged structure, $CH_2(OH)CH_2^+$, which can be described as protonated oxirane,[20–22,28] and CH_3CHOH^+, which is obtained by shifting a hydrogen atom from the central to the terminal carbon atom (Fig. 1). Due to the large geometrical changes which occur upon ionization, only an upper limit to the ionization energy (IE) has been obtained experimentally.[28] Ruscic and Berkowitz[28] derived an adiabatic IE $\leq$ 8.35 eV from their photoion yield curve but suggested that the lower limit might be $\leq$8.18 eV. Based on heat of formation arguments, they proposed an adiabatic IE of 7.78 eV.

Curtiss *et al.*[20] characterized stationary points on the CH_2CH_2OH and $H_5C_2O^+$ ground states, using the G2 method.[29] They identified three structures on the neutral potential energy surface (PES), which they assigned as minima labeled as 3a (C_s), 3b (C_1) and 3c (C_1).[20] They also optimized the cation geometry starting from these three struc-

[a]Present address: Jet Propulsion Laboratory, 4800 Oak Grove Drive, M/S 183-901, Pasadena, CA 91109.
[b]Author to whom correspondence should be addressed. Electronic mail: krylov@usc.edu.

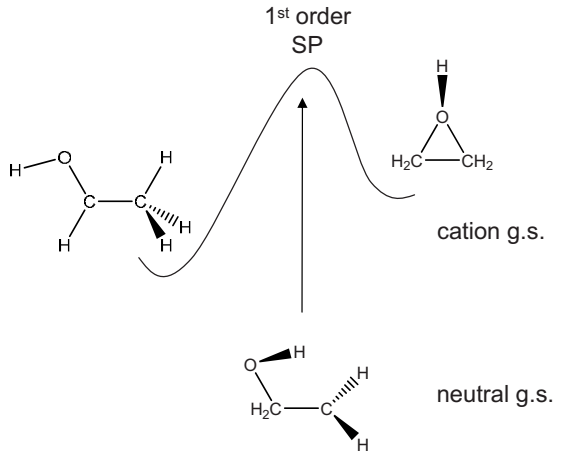

FIG. 1. First ionization of CH_2CH_2OH. On the cation PES there is a first order saddle point in the Franck–Condon region which connects the CH_3CHOH^+ and $CH_2(OH)CH_2^+$ conformers. The calculated vertical and adiabatic IEs are VIE=8.93 eV, AIE=6.21 and 7.37 eV.

tures, and showed that (i) 3a converged to $CH_2(OH)CH_2^+$, (ii) 3b converged without activation energy to CH_3CHOH^+, and (iii) 3c also converged to CH_3CHOH^+.

In the present work, we find only two minima on the ground-state PES, 3b and 3c, which we refer to as M2 and M1 respectively, with M1 denoting the global minimum. In our calculations 3a is a saddle point with a single negative frequency of ~ 100 cm^{-1}. In addition to 3a (referred to below as SP4), we find five other saddle points, which lie within 900 cm^{-1} of M1. The conformers and saddle points differ mostly along two dihedral coordinates, labeled d_{HOCC} (OH torsion around CO), and d_{OCCH} (CH_2 torsion around CC), which are depicted in Fig. 2(a). These two internal rotations give rise to several first-order and second-order saddle points shown in Fig. 2(b), due partly to steric hindrance. We label them as SP1–SP6.

Although the saddle points are not sampled by the ground-state vibrational wave function, they become populated under thermal experimental conditions. Also, these regions of the ground state PES are the only routes leading to cyclization on the cation/Rydberg surfaces. Therefore, we include them in our study.

The cation surface has been studied computationally by Bock *et al.*,[21] who characterized several stationary points of the $CH_2(OH)CH_2^+$ and CH_3CHOH^+ structural isomers at the MP2/6-31G(d) level. In agreement with the results of Curtiss *et al.*[20] and Bock *et al.*,[21] we find no minima in the open-chain, $CH_2CH_2OH^+$ configuration on the $H_5C_2O^+$ surface. Optimizations starting from M1 or M2 converge to CH_3CHOH^+ (Fig. 1, left pathway), while optimizations from various saddle points on the PES of the neutral state lead to either CH_3CHOH^+ or the bridged structure $CH_2(OH)CH_2^+$ (Fig. 1, right pathway).

The information we provide in this paper concerns the excited electronic states of CH_2CH_2OH, and it should be useful in carrying out and interpreting experiments. Specifically, we examine whether the two stable conformers M1 and M2, and the six low-lying saddle points SP1–SP6 exhibit different behaviors upon electronic excitation and ionization. To this end, we characterize their excitation energies, oscillator strengths, and possible dissociation routes. We also identify isomerization products for the unstable open-chain cation and assert that the same behavior can be expected in the Rydberg states of the neutral. In a future publication, we will discuss the vibrational spectroscopy and dynamics on the neutral and cation ground-state PESs.

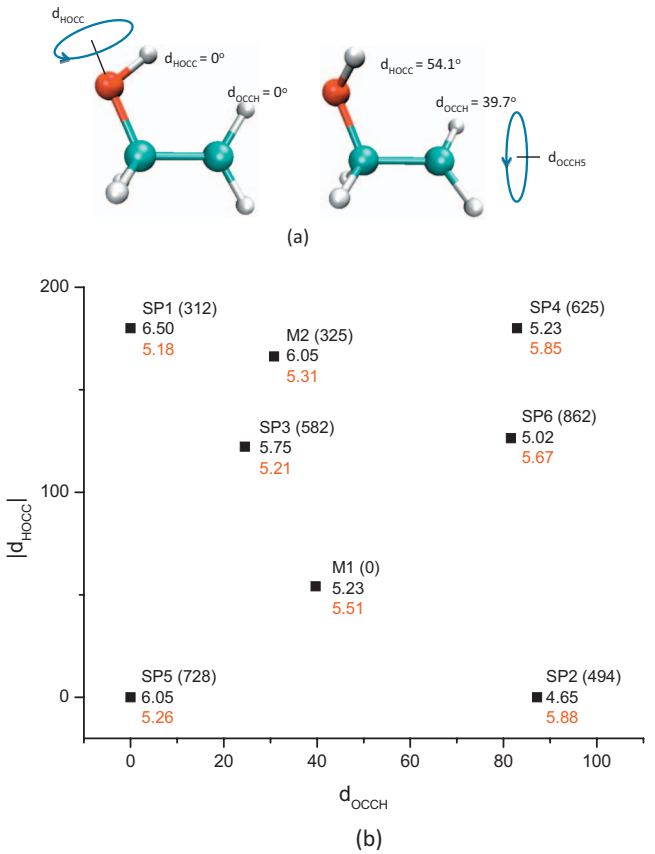

FIG. 2. (a) d_{HOCC} (OH torsion) and d_{OCCH} (CH_2 torsion) are the two major structural differences between the minima and all other stationary points. (b) Geometries of all conformers with respect to $|d_{HOCC}|$ and d_{OCCH}. Parentheses: relative energies on the ground state (cm^{-1}). Middle number: total energy of the (HOMO−1→SOMO) valence state. Lower number (in red): total energy of the SOMO→3s Rydberg state.

The structure of this paper is as follows. Section II discusses computational details, Sec. III describes the geometrical aspects and molecular orbitals on the ground state, Sec. IV considers dissociation on the valence and n=3 Rydberg states and their relationship with the cation, and Sec. V provides the conclusions.

II. COMPUTATIONAL DETAILS

All calculations were performed using the Q-CHEM (Ref. 30) and MOLPRO version 2002.6 (Ref. 31) electronic structure packages. Equilibrium geometries for M1, M2, and SP4 (3a in the work of Curtiss *et al.*)[20] were obtained using the coupled-cluster method with single and double substitutions (CCSD) (Ref. 32) with the 6-311+G(d,p) basis set, and an unrestricted Hartree–Fock reference. This basis set was derived from the polarized split-valence 6-311G(d,p) basis[33,34] by augmenting it with one set of diffuse sp functions on heavy atoms. All optimizations were performed without symmetry constraints. The typical values of $\langle S^2 \rangle$ were around

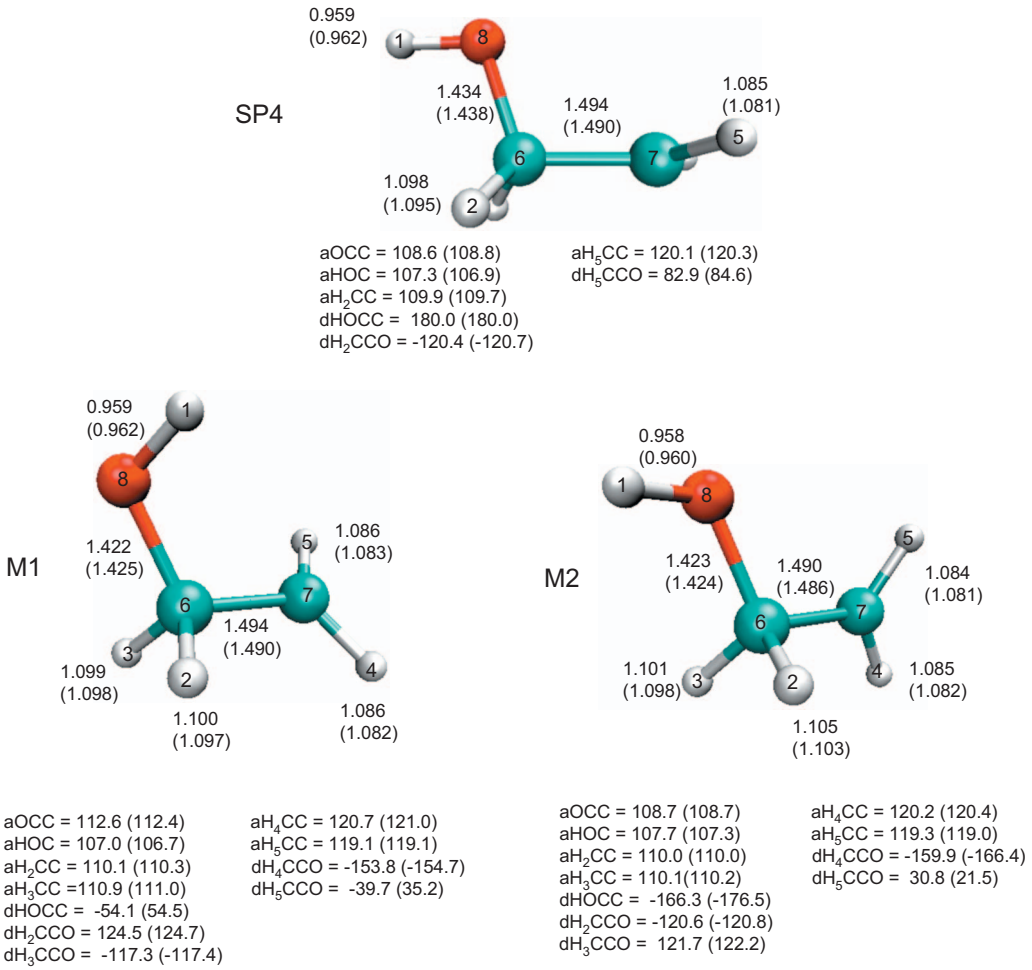

FIG. 3. Equilibrium structures for global minimum M1, local minimum M2, and first order saddle point SP4. Regular print: CCSD/6-311+G(d,p). In parentheses: CCSD(T)/cc-pVTZ optimized full dimensional PES (see text).

0.76 for all ground state calculations. The optimized geometries of neutral CH_2CH_2OH at the CCSD/6-311+G(d,p) level are shown in Fig. 3. Energy ordering of all the conformers was obtained by single-point calculations using the CCSD(T) method[35,36] with the cc-pVQZ (Ref. 37) basis set (Table I). A complete basis set (CBS) extrapolation of the energies was performed using a two point formula of Helgaker *et al.*[38,39] for CCSD(T) with cc-pVXZ basis sets. The conformers ordered according to extrapolated total energies, for X=3 and 4, are also shown in Table I. This formula fits the correlation energy to an exponential form; the Hartree–Fock energy was taken from the higher-cardinal basis set. The average difference between the cc-pVQZ and CBS values was 16 cm^{-1}, and the maximum was 27 cm^{-1}. This close agreement indicates good convergence with respect to polarization with basis set size.

We also calculated full-dimensional PESs for the ground states of CH_2CH_2OH and $H_5C_2O^+$. The neutral PES is a polynomial fit in Morse variables of interatomic distances, fit to approximately 12 000 CCSD(T)/cc-pVTZ (Ref. 37) single point energies. Similarly constructed PESs have been used in several dynamics and spectroscopy studies.[40–48] Details of constructing the symmetrized polynomial basis are given elsewhere.[44] The full details of the PES calculations will be presented in a forthcoming paper. For the neutral surface, the single point energies were calculated in the region of

TABLE I. Energies (cm^{-1}) of the conformers at the CCSD(T)/cc-pVQZ level relative to M1 using CCSD(T)/cc-pVQZ and using a two-point extrapolation formula (cc-pVTZ and cc-pVQZ, see text), values of dihedral angles (deg) (see supporting materials for full geometrical parameters of SP1–SP6), dissociation products on the valence state, and isomerization products on the cation PES.

	M1	M2	SP1	SP2	SP3	SP4	SP5	SP6
ΔE (cc-pVQZ)	0	325	312	494	582	625	728	862
ΔE (CBS)	0	307	285	480	567	618	705	856
d_{HOCC}	−54.1	−166.3	180.0	0.0	−122.2	180.0	0.0	−126.4
d_{OCCH}	−39.7	30.8	0.0	87.2	24.5	82.9	0.0	81.6
Valence dissoc. product	CH_2+CH_2OH	CH_2+CH_2OH	$H+CH_2CHOH$	$OH+C_2H_4$	CH_2+CH_2OH	$OH+C_2H_4$	$H+CH_2CHOH$	$OH+C_2H_4$
Cation Isomeriz. product	CH_3CHOH^+	CH_3CHOH^+	CH_3CHOH^+	$CH_2(OH)CH_2^+$	CH_3CHOH^+	$CH_2(OH)CH_2^+$	CH_3CHOH^+	$CH_2(OH)CH_2^+$

CH_2CH_2OH, and did not include CH_3CHOH or other isomerization products. A preliminary fit was done by selecting several thousand points, e.g., with random deviations from the normal modes, and rotations along d_{HOCC} and d_{OCCH}. The fit was further optimized by adding points to the fit from extensive molecular dynamics trajectories on the PES. All major low-energy dissociation fragments were calculated and added to the fit (at interfragment distance of 50 Å) to ensure correct qualitative asymptotic behavior. Finally, a few thousand very high energy structures (>10 hartree above the global minimum) were included. These were calculated at the B3LYP/cc-pVTZ level, and their energies were shifted according to the average difference between a CCSD(T) and B3LYP data set. A similar procedure was used to fit the cation surface, except that the emphasis was on all isomerization products, and this surface was calculated at the B3LYP/cc-pVTZ level.

The neutral surface was used to compare the geometries of M1, M2, and SP4 with *ab initio* calculations, and to characterize all saddle points on the PES. Other than M1, M2, and SP4 (for comparison with Curtiss *et al.*), all conformer geometries were characterized on the fitted PES only. Stationary points were found by Hessian searches starting from geometries taken from high-energy trajectories (to effectively span the configuration space) as well as an evenly spaced displacement grid along both d_{HOCC} and d_{OCCH}. Other than M1 and M2, no additional minima on the CH_2CH_2OH PES were found.

The cation PES is fitted to B3LYP/cc-pVTZ data and covers the region of $CH_2CH_2OH^+$ as well as CH_3CHOH^+, $CH_2(OH)CH_2^+$, and the radical's dissociation products. We used this surface for classical trajectories starting from the Franck–Condon region of CH_2CH_2OH, in order to characterize the ionization end products. We will report details of the vibrational spectroscopy and dynamics on these PESs in a subsequent publication.

All excited electronic states were computed at the neutral optimized geometries, using the equation-of-motion coupled-cluster method for excitation energies (EOM-EE-CCSD)[49–51] with the 6-311(2+,+)G(d,p) basis set, using restricted open-shell Hartree–Fock (ROHF) references. The character of the states was assigned based on the leading EOM amplitudes and the character of the respective MOs as well as the computed sizes of electron density, i.e., the $\langle X^2\rangle$, $\langle Y^2\rangle$, and $\langle Z^2\rangle$ values (see Ref. 12 regarding assigning Rydberg versus valence character). We found that Rydberg-valence interactions for the states discussed below are small at all the geometries considered, and the states are of either pure Rydberg or valence character. We note that using the ROHF reference is crucial for the correct assignment and that spin contamination of the UHF references results in artificial admixture of Rydberg excitations to the valence states.

The vertical excitation energies were calculated at the neutral geometries of the M1 and M2 conformers. The excited states were computed at the geometries optimized by CCSD (Ref. 32) using the 6-311+G(d,p) basis set. The excited states of SP1–SP6 were calculated at the PES-optimized structures. Geometry optimization of the lowest excited valence state was performed using EOM-EE-CCSD with the 6-311G(d,p) basis set.

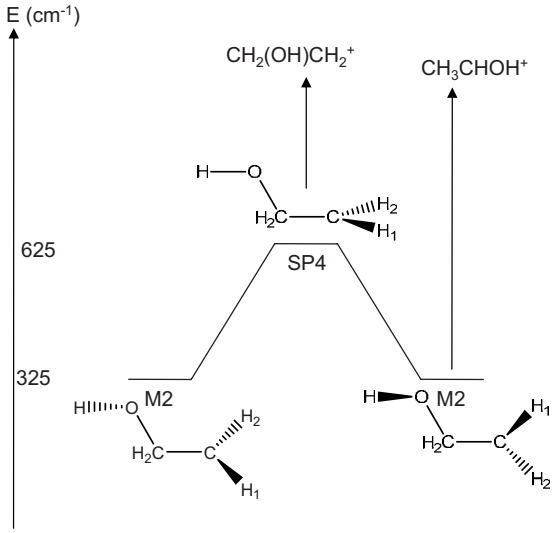

FIG. 4. Torsion along the CH_2 group samples configurations (SP4) that lead to cyclic or linear isomerization products in the cation.

The IEs were computed using EOM-CCSD method for ionized states (EOM-IP-CCSD)[51,52] and CCSD(T). Vertical IEs (VIEs) were obtained using EOM-IP-CCSD/6-311G(d,p). The adiabatic IEs were calculated using CCSD(T)/cc-pVTZ. In addition, the VIE for the M1 structure was computed by CCSD(T)/cc-pVTZ. Optimized geometries of the cation for the IE calculations were obtained using CCSD/6-311+G(d,p).

III. GROUND STATE CONFORMATIONS

We characterized two minima and six saddle points on the CH_2CH_2OH PES. All lie within 900 cm^{-1} of the global minimum. These saddle points arise from steric interactions upon torsion of the terminal CH_2 and OH bonds. They are labeled SP1–SP6 in order of increasing single point energy at the CCSD(T)/cc-pVQZ and CBS levels (Table I) at the CCSD(T)/cc-pVTZ fitted PES geometries.

M1 and M2 are connected by SP3 (582 cm^{-1} above M1). The value of d_{HOCC} for SP3 is intermediate between M1 and M2. The value of d_{OCCH} for SP3 is much closer to that of M2 than of M1 [Fig. 2(b), Table I]. The M1→M2 minimum energy pathway must go around a barrier to OH torsion that exists around the configurational space of M1.

M1, M2, and SP4 (equivalent to 3a of Curtiss *et al.*)[20] are shown also in Fig. 3 at the CCSD/6-311+G(d,p) and PES geometries, along with all geometrical parameters. We find that SP4 is a saddle point connecting mirror images of M2 along d_{OCCH} (Fig. 4), and its ionization is one of the channels leading to isomerization to the cyclic $CH_2(OH)CH_2^+$ on the cation surface (see Fig. 4) (similar behavior is expected for the Rydberg state). The relative energies and values of d_{HOCC} and d_{OCCH} are provided in Table I for the ground electronic state of all the other saddle points; full geometrical parameters for these saddle points are provided in supplementary materials.[53]

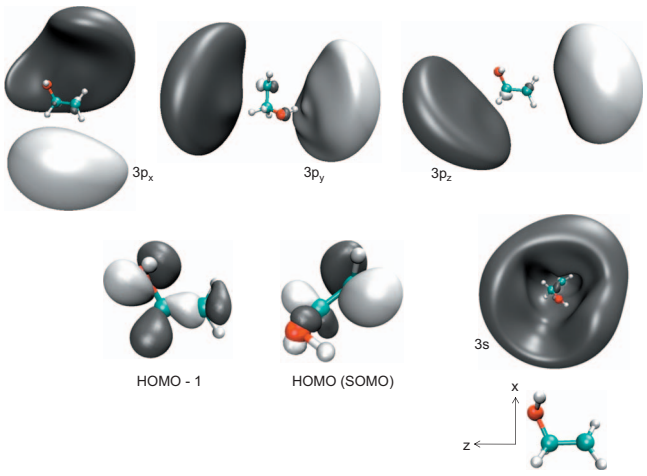

FIG. 5. Relevant molecular orbitals involved in the lowest valence and Rydberg transitions.

The equilibrium structures at CCSD/6-311+G(d,p) and on our fitted PES are in good agreement with each other for M1, M2, and SP4. For all three structures, bond lengths are within 0.004 Å; CCSD(T)/cc-pVTZ predicts a slightly shorter CC bond and slightly longer CO and OH bonds than CCSD/6-311+G(d,p). Angles are also within 0.5° between the two methods. A larger discrepancy is seen in the dihedral angles for M2, where CCSD(T) predicts a more planar structure. The HOCC dihedral angle is larger by 10.2°, and the OCCH dihedral angle is smaller by 9.3° relative to CCSD/6-311+G(d,p). We find that the differences are due to the extremely flat PES in this region.

IV. ELECTRONIC EXCITATIONS AND IONIZATION

The molecular orbitals involved in the lowest transitions are shown in Fig. 5 for the M1 conformer. The orbitals of the other conformers and saddle points have similar character. The highest occupied molecular orbital (HOMO) is singly occupied, and is mostly an atomic p-orbital on the terminal carbon. It also has density on the two sigma-CH bonds of the central carbon, providing an antibonding interaction along the CC bond. We refer henceforth to this orbital as the SOMO. The HOMO-1 is doubly occupied. It is mostly an atomic p-orbital on oxygen, oriented perpendicular to the HOC plane. It has antibonding character along the CO and it is bonding along CC. The 3s and $3p_{x,y,z}$ Rydberg orbitals (Fig. 5) differ very little for all eight conformers and saddle points.

Table II includes calculated VIEs from all of the neutral conformers and saddle points. The CCSD(T)/cc-pVTZ VIE for M1 is 8.93 eV and the two adiabatic IEs are 6.21 and 7.37 eV corresponding to the hydrogen-transferred and cyclic structures, respectively. The significant geometry changes upon ionization result in poor Franck–Condon factors, preventing direct adiabatic photoionization from the ground vibrational state of the neutral. Indeed, the observed experimental upper bound of the adiabatic IE $\leq$ 8.35 eV (or 8.11 eV) derived from the photoionization efficiency curves[28] lies between the calculated adiabatic and vertical IEs. It corresponds, most likely, to the lowest energy state with sufficient Franck–Condon factor to be experimentally detected. Examination of molecular dynamics trajectories on the cation ground-state reveals fast isomerization from the neutral equilibrium geometry to one of the stable cation minima (Fig. 1).

The vertical electronic excitation energies and oscillator strengths for all conformers and saddle points are given in Table II and the energies are also displayed in Figs. 6(a) and 6(b). Figure 6(a) shows schematically the energies of the excited states of M1 and M2, and Fig. 6(b) compares the VIEs with the energies of the excited Rydberg states for all conformers and saddle points. In all cases the lowest excitation is to either of two states: the valence (HOMO−1 → SOMO) state or the Rydberg (SOMO → 3s) state, and the excitation energy of the lowest transitions is spread between 4.65 and 5.31 eV (267–233 nm) (Table II). In four of the structures (conformers or saddle points) the Rydberg state is the lowest excited state; in the remaining four, the valence state is the lowest. The largest oscillator strength from M1 is to the 3s state, whereas in M2 the transition strength is spread more evenly over several excited states. The transition to 3s is usually the strongest, except in SP5, where transition to the lowest valence state is also bright. The proximity of several excited states raises the possibility of surface crossings, but these have not been explored in this work.

Figures 2(a) and 7 show how d_{HOCC} and d_{OCCH} affect the energies of the valence and 3s excited states. The energy of the valence state is the most sensitive to conformer geometry, and it decreases continuously with decreasing d_{HOCC} [moving down the chart in Fig. 2(b)] and increasing d_{OCCH} (moving to the right). The 3s Rydberg state energy increases at larger d_{OCCH} and is lowest in energy when $d_{HOCC} \sim 120°$. To highlight the dependence on d_{HOCC}, Fig. 7 displays the ener-

TABLE II. Excitation and IEs (eV) and oscillator strengths (in parentheses) for different conformers and saddle points of CH_2CH_2OH.

	M1	M2	SP1	SP2	SP3	SP4	SP5	SP6
Valence	5.23 (0.004)	6.05 (0.010)	6.50 (0.013)	4.65 (0.0007)	5.75 (0.003)	5.22 (0.0005)	6.05 (0.019)	5.02 (0.003)
SOMO→3s	5.51 (0.028)	5.31 (0.011)	5.18 (0.007)	5.88 (0.032)	5.21 (0.012)	5.83 (0.028)	5.26 (0.017)	5.67 (0.030)
SOMO→$3p_x$	6.29 (0.004)	6.17 (0.011)	5.72 (0.011)	6.75 (0.004)	6.04 (0.007)	6.89 (0.003)	5.94 (0.004)	6.63 (0.0004)
SOMO→$3p_y$	6.48 (0.007)	6.29 (0.006)	6.11 (0.018)	6.78 (0.002)	6.29 (0.005)	6.65 (6e-5)	6.32 (0.013)	6.56 (0.002)
SOMO→$3p_z$	6.31 (0.008)	5.85 (0.013)	6.08 (0.007)	6.89 (0.007)	5.83 (0.018)	6.49 (0.014)	6.19 (0.001)	6.33 (0.004)
VIE[a]	8.98	8.66	8.53	9.39	8.62	9.17	8.79	9.06

[a]EOM-IP-CCSD/6-311G(d,p).

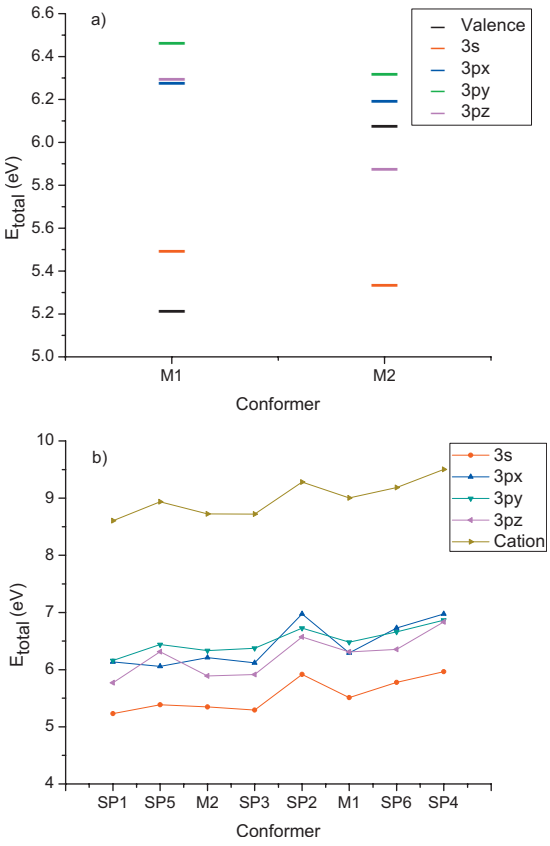

FIG. 6. (a) Excited state total energies for the two stable conformers. (b) Comparison of Rydberg state vertical energies for all conformers. The cation VIE is also plotted for comparison. All energies are relative to M1.

gies of these two states in groups of similar values of d_{OCCH}, where the ordering on the *x*-axis correlates with a decrease in d_{HOCC}.

Based on the energy of these two states, we predict that excitation with ~5 eV photons would lead to dynamics on either the 3s or the valence state depending on the starting conformation. Previous experiments have shown that moderately strong one-photon absorption occurs at 266 nm (4.66 eV).[23,25,26]

It is also noteworthy that the Rydberg-state energy curves shown in Fig. 6(b) are almost parallel to the cation energy curve, especially for the 3s and out-of-plane $3p_y$ states. This suggests that the dynamics on the Rydberg PESs will be similar to that on the cation PES, and that the interaction of the Rydberg electron with the ionic core is weak. Therefore, in order to predict the dynamics on the neutral Rydberg surfaces, we explored isomerization pathways for the cation (see Sec. IV A). In addition, we find that the valence state is repulsive and dissociative, as described further in Sec. IV B.

Following initial excitation to either the HOMO−1 → SOMO or the SOMO → 3s state the radical may (i) dissociate on the valence state or (ii) isomerize on the Rydberg state. It is also possible that during movement along either of these surfaces, crossings between the two states and/or with the ground state will occur. The isomerization and dissociation pathways are described further below.

A. Isomerization on the cation and Rydberg surfaces

As discussed above, isomerization on the Rydberg PESs should be similar to the corresponding isomerization in the cation. To identify the isomerization products we placed each conformer on the cation PES with no initial kinetic energy and run classical MD trajectories. Since vertical ionization does not access stationary points on the cation PES, fast isomerization (within several vibrational periods) was observed. All the conformers isomerized either to CH_3CHOH^+ or to the cyclic $CH_2(OH)CH_2^+$, with the end product depending on the initial orientation of the CH_2 group in the neutral radical. Geometry optimizations of the cation, starting from conformer geometries and using B3LYP/6-311G(2df,p), yielded the same end products as the MD trajectories. The gradients on the cation surface in the Franck–Condon regions are fairly steep, and adding classical kinetic energy equivalent to the zero-point energy (partitioned randomly along the normal modes) to the initial conditions for the trajectories did not change the isomerization results.

Ionization to the ground state of the cation is well described by removing an electron from the SOMO, which is primarily a p-orbital on the terminal carbon oriented perpendicular to the CH_2 plane. We find that when $d_{OCCH} \sim 90°$, only the cyclic ion structure is produced regardless of OH orientation. If the lobes of the empty p-orbital are oriented toward the oxygen, as when $d_{OCCH} \sim 90°$, then the ion cyclizes easily to form $CH_2(OH)CH_2^+$. However, if d_{OCCH} is in the range 0°–40° (Table I) then the p-orbital lobes are ori-

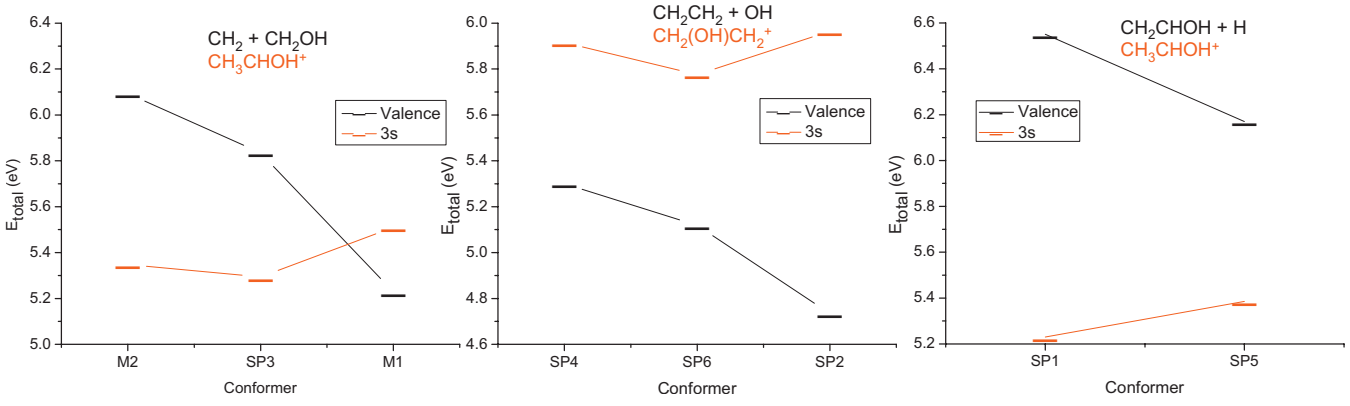

FIG. 7. Comparison of excited state energies and dissociation products on the valence state (black) and Rydberg 3s state (red). See also Fig. 2(a) and the text.

ented parallel to the central carbon CH bonds. At the same time, the electrons on the oxygen are blocked from closing the ring by a terminal CH bond, and the radical undergoes a hydrogen shift to the linear CH_3CHOH^+ cation, whose adiabatic IE from its neutral form is low (6.64 eV).[54] The optimized geometries of M1 and M2 have $d_{OCCH}=39.7°$ and 30.8°, respectively, and therefore they isomerize to the linear structure, as well as SP1, SP3, and SP5. The saddle point geometries that converge to $CH_2(OH)CH_2^+$ are SP4, SP2, and SP6, which have $d_{OCCH}=82.9°$, 87.2°, and 81.6°, respectively. The isomerization outcomes on the cation PES are summarized in Table I and are also shown in Fig. 7, grouped by approximate d_{OCCH}. As discussed above, we expect the Rydberg states to exhibit similar behavior to that of the cation.

Because of the large difference in equilibrium geometries between the ground and Rydberg electronic states, it is hard to predict the adiabatic onset of the absorption. When calculating the energies of the 3s state at the equilibrium geometries of the cation's isomers, the energy difference between CH_3CHOH and $CH_2(OH)CH_2$ agrees with that in the cation [CH_3CHOH is lower than $CH_2(OH)CH_2$ by 1.3 eV on the cation PES and by 1.9 eV on the Rydberg PES]. The lowest adiabatic excitation energy corresponds to a transition to the 3s state at its optimized CH_3CHOH geometry, with $E_{ex}\sim 2.5$ eV. In the calculation we have not optimized this geometry; instead we used the cation optimized structures. However, such adiabatic excitation may not be easily accessible from the ground state of the neutral because of the extensive nuclei rearrangement required for $CH_2CH_2OH \rightarrow CH_3CHOH$ isomerization. The Rydberg states of CH_3CHOH are known to couple efficiently with the ground state,[3] and thus fast dissociation on the ground state PES may follow isomerization on the Rydberg state to CH_3CHOH and give rise to H photofragments by fission of the OH and CH bonds.[3]

B. Dissociation on the valence state

The lowest valence state is derived from the HOMO $-1 \rightarrow$ SOMO excitation. It corresponds to removing an electron from an orbital with bonding character along CC and placing it in an orbital with antibonding character along CC, thereby doubly destabilizing the CC bond. We thus expect the valence state to be repulsive, and we characterized the dissociation products by geometry optimizations starting from each conformer and saddle point.

We find that three dissociation channels on the valence state are feasible and that they correlate with specific dihedral angles d_{OCCH}. The three conformers that dissociate to CH_2+CH_2OH have $d_{OCCH}\sim 0°-40°$ (M1, M2, SP3; $d_{OCCH}=39.7°$, 30.8°, and 24.5°, respectively). The three that dissociate to CH_2CH_2+OH have $d_{OCCH}\sim 90°$ (SP4, SP2, SP6; $d_{OCCH}=82.9°$, 87.2°, and 81.6°, respectively). The SP1 and SP5 conformers both have $d_{OCCH}=0°$, and $d_{HOCC}=0°$ or 180°, and they dissociate to $H+CH_2CHOH$. The valence state dissociation products for all conformers are listed in Table I and shown in Fig. 7.

V. CONCLUSIONS

The energies of the excited electronic states and oscillator strengths for transitions to Rydberg and valence states of CH_2CH_2OH were calculated for two stable conformers, M1 and M2, and six low-lying saddle points, SP1–SP6. A dense manifold of low-lying electronic states was found at 5–7 eV consisting of close-lying valence and Rydberg states and leading to rich and complex dissociation and isomerization dynamics. The two lowest-lying states derive from HOMO $-1 \rightarrow$ SOMO and SOMO $\rightarrow$ 3s excitations and their relative order depends sensitively on the dihedral angles d_{OCCH} and d_{HOCC}.

Excitation to the Rydberg states leads, similarly to the cation, to isomerization to either CH_3CHOH or the cyclic $CH_2(OH)CH_2$ depending on conformer or saddle point geometry. The valence state is repulsive, and its dissociation should be prompt and can proceed along the CC, CO, and CH bonds leading to CH_2+CH_2OH, CH_2CH_2+OH, and $H+CH_2CHOH$, respectively. Surface crossings among Rydberg and valence states and the ground state are likely to affect dissociation as well. We thus expect the absorption spectrum at 5–7 eV to be featureless. The small conformational barriers on the neutral PES (300–900 cm^{-1}) lead to population of several conformers and saddle points, which give rise, in turn, to different dynamics and dissociation outcomes on the excited state PESs.

ACKNOWLEDGMENTS

This work was conducted under the auspices of the iOpenShell Center for Computational Studies of Electronic Structure and Spectroscopy of Open-Shell and Electronically Excited Species supported by the National Science Foundation through Grant No. CRIF:CRF CHE-0625419 +0624602+0625237. A.I.K. and H.R. also acknowledge support of the Department of Energy (Grant Nos. DE-FG02-05ER15685 and DE-FG02-05ER15629, respectively)

[1] C. A. Taatjes, N. Hansen, A. McIlroy, J. A. Miller, J. P. Senosiain, S. J. Klippenstein, F. Qi, L. Sheng, Y. Zhang, T. A. Cool, J. Wang, P. R. Westmoreland, M. E. Law, T. Kasper, and K. Kohse-Höinghaus, Science **308**, 1887 (2005).
[2] J. P. Senosiain, S. J. Klippenstein, and J. A. Miller, J. Phys. Chem. A **110**, 6960 (2006).
[3] B. Karpichev, L. W. Edwards, J. Wei, and H. Reisler, J. Phys. Chem. A **112**, 412 (2008).
[4] L. Feng, A. V. Demyanenko, and H. Reisler, J. Chem. Phys. **120**, 6524 (2004).
[5] L. Feng, A. V. Demyanenko, and H. Reisler, J. Chem. Phys. **118**, 9623 (2003).
[6] L. Feng, X. Huang, and H. Reisler, J. Chem. Phys. **117**, 4820 (2002).
[7] L. Feng and H. Reisler, J. Phys. Chem. A **108**, 9847 (2004).
[8] V. Aristov, D. Conroy, and H. Reisler, Chem. Phys. Lett. **318**, 393 (2000).
[9] D. Conroy, V. Aristov, L. Feng, and H. Reisler, J. Phys. Chem. A **104**, 10288 (2000).
[10] B. C. Hoffman and D. R. Yarkony, J. Chem. Phys. **116**, 8300 (2002); D. R. Yarkony, *ibid.* **122**, 084316 (2005).
[11] B. Karpichev, H. Reisler, A. I. Krylov, and K. Diri, J. Phys. Chem. A **112**, 9965 (2008).
[12] H. Reisler and A. I. Krylov, Int. Rev. Phys. Chem. **28**, 267 (2009).
[13] F. P. Tully, Chem. Phys. Lett. **143**, 510 (1988).
[14] P. A. Cleary, M. T. B. Romero, M. A. Blitz, D. E. Heard, M. J. Pilling, P. W. Seakins, and L. Wang, Phys. Chem. Chem. Phys. **8**, 5633 (2006) (and references therein).

[15] H. Hippler and B. Viskolcz, Phys. Chem. Chem. Phys. **2**, 3591 (2000).
[16] A. B. Vakhtin, J. E. Murphy, and S. R. Leone, J. Phys. Chem. A **107**, 10055 (2003).
[17] C. Sosa and H. B. Schlegel, J. Am. Chem. Soc. **109**, 7007 (1987); **109**, 4193 (1987).
[18] E. W. G. Diau and Y. P. Lee, J. Chem. Phys. **96**, 377 (1992).
[19] T. Yamada, J. W. Bozzelli, and J. Lay, J. Phys. Chem. A **103**, 7646 (1999).
[20] L. A. Curtiss, D. J. Lucas, and J. A. Pople, J. Chem. Phys. **102**, 3292 (1995).
[21] C. W. Bock, P. George, and J. P. Glusker, J. Org. Chem. **58**, 5816 (1993).
[22] R. H. Nobes, W. R. Rodwell, W. J. Bouma, and L. Radom, J. Am. Chem. Soc. **103**, 1913 (1981).
[23] C. Anastasi, V. Simpson, J. Munk, and P. Pagsberg, J. Phys. Chem. **94**, 6327 (1990).
[24] E. J. Hintsa, X. S. Zhao, and Y. T. Lee, J. Chem. Phys. **92**, 2280 (1990).
[25] V. A. Shubert, M. Rednic, and S. T. Pratt, J. Phys. Chem. A **113**, 9057 (2009).
[26] S. P. Sapers and W. P. Hess, J. Chem. Phys. **97**, 3126 (1992).
[27] D. W. Chandler, J. W. Thoman, and W. P. Hess, Inst. Phys. Conf. Ser. **114**, 355 (1991).
[28] B. Ruscic and J. Berkowitz, J. Chem. Phys. **101**, 10936 (1994).
[29] L. A. Curtiss, K. Raghavachari, G. W. Truks, and J. A. Pople, J. Chem. Phys. **94**, 7221 (1991).
[30] Y. Shao, L. F. Molnar, Y. Jung, J. Kussmann, C. Ochsenfeld, S. Brown, A. T. B. Gilbert, L. V. Slipchenko, S. V. Levchenko, D. P. O'Neil, R. A. Distasio, Jr., R. C. Lochan, T. Wang, G. J. O. Beran, N. A. Besley, J. M. Herbert, C. Y. Lin, T. Van Voorhis, S. H. Chien, A. Sodt, R. P. Steele, V. A. Rassolov, P. Maslen, P. P. Korambath, R. D. Adamson, B. Austin, J. Baker, E. F. C. Bird, H. Daschel, R. J. Doerksen, A. Drew, B. D. Dunietz, A. D. Dutoi, T. R. Furlani, S. R. Gwaltney, A. Heyden, S. Hirata, C.-P. Hsu, G. S. Kedziora, R. Z. Khalliulin, P. Klunziger, A. M. Lee, W. Z. Liang, I. Lotan, N. Nair, B. Peters, E. I. Proynov, P. A. Pieniazek, Y. M. Rhee, J. Ritchie, E. Rosta, C. D. Sherrill, A. C. Simmonett, J. E. Subotnik, H. L. Woodcock III, W. Zhang, A. T. Bell, A. K. Chakraborty, D. M. Chipman, F. J. Keil, A. Warshel, W. J. Herhe, H. F. Schaefer III, J. Kong, A. I. Krylov, P. M. W. Gill, and M. Head-Gordon, Phys. Chem. Chem. Phys. **8**, 3172 (2006).
[31] MOLPRO is a package of *ab initio* programs written by H.-J. Werner, P. J. Knowles, R. Lindh, F. R. Manby, M. Schütz, P. Celani, T. Korona, A. Mitrushenkov, G. Rauhut, T. B. Adler, R. D. Amos, A. Bernhardsson, A. Berning, D. L. Cooper, M. J. O. Deegan, A. J. Dobbyn, F. Eckert, E. Goll, C. Hampel, G. Hetzer, T. Hrenar, G. Knizia, C. Köppl, Y. Liu, A. W. Lloyd, R. A. Mata, A. J. May, S. J. McNicholas, W. Meyer, M. E. Mura, A. Nicklass, P. Palmieri, K. Pflüger, R. Pitzer, M. Reiher, U. Schumann, H. Stoll, A. J. Stone, R. Tarroni, T. Thorsteinsson, M. Wang, and A. Wolf.
[32] G. D. Purvis and R. J. Bartlett, J. Chem. Phys. **76**, 1910 (1982).
[33] R. Krishnan, J. S. Binkley, R. Seeger, and J. A. Pople, J. Chem. Phys. **72**, 650 (1980).
[34] A. D. McLean and G. S. Chandler, J. Chem. Phys. **72**, 5639 (1980).
[35] K. Raghavachari, G. W. Trucks, J. A. Pople, and M. Head-Gordon, Chem. Phys. Lett. **157**, 479 (1989).
[36] J. D. Watts, J. Gauss, and R. J. Bartlett, J. Chem. Phys. **98**, 8718 (1993).
[37] T. H. Dunning, J. Chem. Phys. **90**, 1007 (1989).
[38] A. Halkier, T. Helgaker, P. Jørgensen, W. Klopper, H. Koch, J. Olsen, and A. K. Wilson, Chem. Phys. Lett. **286**, 243 (1998).
[39] K. L. Bak, P. Jørgensen, J. Olsen, T. Helgaker, and W. Klopper, J. Chem. Phys. **112**, 9229 (2000).
[40] A. Brown, B. J. Braams, K. M. Christoffel, Z. Jin, and J. M. Bowman, J. Chem. Phys. **119**, 8790 (2003).
[41] X. Huang, B. J. Braams, S. Carter, and J. M. Bowman, J. Am. Chem. Soc. **126**, 5042 (2004).
[42] A. Brown, A. B. McCoy, B. J. Braams, Z. Jin, and J. M. Bowman, J. Chem. Phys. **121**, 4105 (2004).
[43] S. C. Park, B. J. Braams, and J. M. Bowman, J. Theor. Comput. Chem. **4**, 163 (2005).
[44] X. Huang, B. J. Braams, and J. M. Bowman, J. Chem. Phys. **122**, 044308 (2005).
[45] X. Huang, B. J. Braams, and J. M. Bowman, J. Phys. Chem. A **110**, 445 (2006).
[46] Z. Xie, B. J. Braams, and J. M. Bowman, J. Chem. Phys. **122**, 224307 (2005).
[47] L. Koziol, V. A. Mozhayskiy, B. J. Braams, J. M. Bowman, and A. I. Krylov, J. Phys. Chem. A **113**, 7802 (2009).
[48] L. Koziol, Y. Wang, B. J. Braams, J. M. Bowman, and A. I. Krylov, J. Chem. Phys. **128**, 204310 (2008).
[49] H. Koch, H. J. Aa. Jensen, P. Jørgensen, and T. Helgaker, J. Chem. Phys. **93**, 3345 (1990).
[50] J. F. Stanton and R. J. Bartlett, J. Chem. Phys. **98**, 7029 (1993).
[51] A. I. Krylov, Annu. Rev. Phys. Chem. **59**, 433 (2008).
[52] D. Sinha, D. Mukhopadhyay, and D. Mukherjee, Chem. Phys. Lett. **129**, 369 (1986); J. F. Stanton and J. Gauss, J. Chem. Phys. **111**, 8785 (1999); P. A. Pieniazek, S. E. Bradforth, and A. I. Krylov, *ibid.* **129**, 074104 (2008).
[53] See supplementary material at http://dx.doi.org/10.1063/1.3354975 for pictures and geometrical parameters of all saddle points. A file with their xyz coordinates, including the minima M1 and M2 is also provided.
[54] J. M. Dyke, A. P. Groves, E. P. F. Lee, and M. H. Z. Niavaran, J. Phys. Chem. A **101**, 373 (1997).